Geophys. J. Int. (2003) **154,** 957–969

Electric and magnetic galvanic distortion decomposition of tensor CSAMT data. Application to data from the Buchans Mine (Newfoundland, Canada)

Xavier Garcia,[1,*] David Boerner[2] and Laust B. Pedersen[3]

[1] *Woods Hole Oceanographic Institution,* MS#7, *Woods Hole* 02543, *USA. E-mail: xavi@whoi.edu*
[2] *Geological Survey of Canada,* 615 *Booth St, Ottawa, Ontario,* K1A 0E9, *Canada*
[3] *Uppsala University, Department of Earth Sciences, Villavägen* 16, *Uppsala,* SE-752 36, *Sweden*

Accepted 2003 April 16. Received 2003 April 16; in original form 2002 June 5

SUMMARY

We have developed a Marquardt–Levenberg inversion algorithm incorporating the effects of near-surface galvanic distortion into the electromagnetic (EM) response of a layered earth model. Different tests on synthetic model responses suggest that for the grounded source method, the magnetic distortion does not vanish for low frequencies. Including this effect is important, although to date it has been neglected. We have inverted 10 stations of controlled-source audio-magnetotellurics (CSAMT) data recorded near the Buchans Mine, Newfoundland, Canada. The Buchans Mine was one of the richest massive sulphide deposits in the world, and is situated in a highly resistive volcanogenic environment, substantially modified by thrust faulting. Preliminary work in the area demonstrated that the EM fields observed at adjacent stations show large differences due to the existence of mineralized fracture zones and variable overburden thickness. Our inversion results suggest a three-layered model that is appropriate for the Buchans Mine. The resistivity model correlates with the seismic reflection interpretation that documents the existence of two thrust packages. The distortion parameters obtained from the inversion concur with the synthetic studies that galvanic magnetic distortion is required to interpret the Buchans data since the magnetic component of the galvanic distortion does not vanish at low frequency.

Key words: Buchans Mine, controlled-source audiomagnetotellurics, galvanic distortion.

1 INTRODUCTION

Controlled-source audiofrequency magnetotellurics (CSAMT) is an electromagnetic (EM) exploration method that was developed in the early 1970s because the sensors and instrumentation of the day were not adequate for detecting the weak natural signals used in the magnetotelluric (MT) sounding method (Strangway *et al.* 1973). The CSAMT method uses an artificial source to generate electromagnetic fields, thereby avoiding the unpredictable behaviour of natural EM fields.

In CSAMT data we can recognize three period bands. The first band, at short periods, and for a layered earth, is called the *far field* where the source EM fields are planar. In this case the electric and magnetic fields measured over a layered earth are equivalent to those measured with natural sources. The CSAMT data in this *far-field* region depend on the source, the distance between the source and the receiver and the resistivity distribution of the earth, and it is only defined for a layered earth. The long-period band is called the *near field*. Here the impedance and tipper vector become real and frequency independent. Between these two regions there is a *transition zone* characterized by a fast variation of the EM fields with frequency.

Galvanic distortion is caused by charge accumulations on conductivity gradients and the superposition of local electric and magnetic anomalous fields on the regional response from large-scale structures. The distortion responses can be classified as electric and magnetic depending on the local field that generates it. The electric field distortion response is frequency independent while the magnetic field is related to frequency, and for this reason galvanic electric distortion is easier to detect and compensate for than galvanic magnetic distortion. Galvanic magnetic distortion is often neglected because it only affects the higher frequencies for plane-wave responses, usually vanishing in the frequency range appropriate to geophysical prospecting. At periods in which a significant part of the induction currents are affected by inhomogeneities, galvanic magnetic distortion is important. Singer (1992) reviewed the circumstances that control its importance, although many authors have ignored the problem of magnetic distortion. Zonge & Hughes (1991), for example, examine electric galvanic distortion for the CSAMT method

*Formerly at the Geological Survey of Canada.

and show field data that is clearly affected by distortion, but exclude any mention to magnetic galvanic distortion. Zhang *et al.* (1993) discuss the distortion in the vertical transfer functions due to electric galvanic effects, but they neglect the magnetic galvanic contribution. Chave & Smith (1994) developed a theoretical perspective for the electric and magnetic galvanic distortion, and they evaluated their effects on 2-D MT transfer functions. They also showed strong evidence of magnetic galvanic distortion on MT data from the Canadian Shield and northeast Pacific. This theoretical study shows that only the diagonal elements of the magnetic distortion matrix can be recovered from the MT impedance. The off-diagonal parameters can be recovered only if the site gain and the anisotropy are known. Following that work, Smith (1997) derived a different system of equations that has an analytic solution for one single frequency, instead of from a range of frequencies as was suggested by Chave & Smith (1994). Most of the work to date has considered only plane-wave source fields. Maybe because most CSAMT studies have been realized on sedimentary areas that are not severely affected by galvanic distortion, the study of magnetic distortion for controlled source methods has been limited to the theoretical case study of Qian & Pedersen (1992) and the anisotropic case of Li *et al.* (2000).

CSAMT data collected in very resistive environments, such as shields, are severely affected by galvanic distortion. While analysing this type of data, we discovered significant problems arising not only from electric galvanic distortion but also from magnetic field distortion. In order to account for this effect we developed an inversion algorithm that explicitly includes distortion in the forward calculation of the layered earth response. Our inversion algorithm is based on a weighted least-squares solution of the non-linear inverse problem, as described in detail by Pedersen & Rasmussen (1989). This algorithm has been extended to work with controlled source EM data and permits the calculation of both the galvanic horizontal and vertical magnetic distortion parameters. We assume that the data set can be accounted for by a layered, or 1-D, earth.

We present two examples of application of this methodology. First, we use synthetic data obtained with an EM modelling code, consisting in a layered earth in which there is embedded an elongated conductor causing galvanic distortion (Fig. 1). Using this data we test the validity of our model, recovering the model and galvanic distortion parameters. For the second example, the CSAMT survey line 14 (L-14) acquired at the Buchans Mine was inverted to recover distortion parameters and the regional layered earth model. Complementary electromagnetic (line 15, Boerner *et al.* 1993a) and seismic (Thurlow *et al.* 1992) soundings were originally carried out in profiles in the mine surroundings to better understand the local structures within the Buchans group. For the CSAMT survey an 'L'-shaped transmitter configuration was used, consisting of two approximately orthogonal electric bipoles (see Fig. 4 in Section 5). This source was used for both CSAMT survey lines 14 (this work) and 15 (Boerner *et al.* 1993b). Details of the field campaign can be found in Boerner *et al.* (1993a). CSAMT data from line 15 were interpreted by Boerner *et al.* (1993b) using a strategy based on inverting polarization ellipses data from one of the source bipoles. In the present work we obtain the classic impedance tensor using the fact that fields from two orthogonal source polarizations were available. As the distance from the source to the receivers (approximately 9 km, Fig. 4) is larger than four times the bipole lengths (∼2 km), the sources can be considered dipoles (Li & Pedersen 1991). For the same reason we also consider that the centre of the bipoles are coincident. Then, using our new algorithm, the data has been inverted and interpreted.

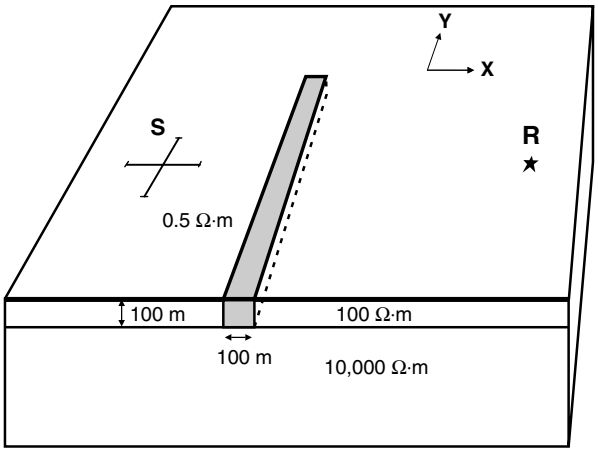

Figure 1. 1-D synthetic model with a 3-D embedded distortion body (grey). *S*, source; *R*, receiver or station.

2 GALVANIC DECOMPOSITION

Small-scale electrical conductivity structures local to the receiver and/or transmitter can distort EM data, making it impossible to know the amplitude of the electric field that represents the response of the bulk earth. It is generally assumed that the magnetic field response of galvanic distortion can be neglected at sufficiently low frequencies. However, this assumption is not proven for tensor CSAMT work and in the present study we have decomposed the impedance tensor into three matrices: one corresponding to the distortion of the electric field, a second for the distortion of the magnetic field and the third representing the regional (1-D) impedance. In the same fashion the transfer function corresponding to the vertical magnetic field has been decomposed into local and regional field components (Wannamaker *et al.* 1984; Zhang *et al.* 1987). The expressions of the measured impedance (complex matrix $\boldsymbol{Z}$) and the tipper vector (complex vector (A, B)) can be expressed after this decomposition as

$$\boldsymbol{Z} = (\mathbf{I} + \mathbf{P}_h)\mathbf{Z}^0 \left(\mathbf{I} + \mathbf{Q}_h \mathbf{Z}^0\right)^{-1} \tag{1}$$

$$(A, B) = \left[(A^0, B^0) + (Q_{zx}, Q_{zy})\mathbf{Z}^0\right] \left(\mathbf{I} + \mathbf{Q}_h \mathbf{Z}^0\right)^{-1}, \tag{2}$$

where the superscript 0 denotes the regional (i.e. undistorted) values of the transfer functions, $\mathbf{I}$ is the identity matrix, $\mathbf{P}_h$ the electric field real galvanic distortion matrix, $\mathbf{Q}_h$ the horizontal magnetic real galvanic distortion matrix and $\mathbf{Q}_z$ the vertical magnetic field real galvanic distortion vector. To represent the magnetic distortion parameters we have used the complex function R_{ij} defined as:

$$R_{ij} = \left(\mathbf{Q}_h \cdot \mathbf{Z}^0\right)_{ij} \tag{3}$$

Note that this function is frequency dependent and can be interpreted as an equivalent galvanic magnetic distortion. In matrix notation the three real distortion matrices are expressed as

$$\begin{aligned} \boldsymbol{P} &= \begin{pmatrix} P_{xx} & P_{xy} \\ P_{yx} & P_{yy} \end{pmatrix} \\ \mathbf{Q}_h &= \begin{pmatrix} Q_{xx} & Q_{xy} \\ Q_{yx} & Q_{yy} \end{pmatrix} \\ \mathbf{Q}_z &= (Q_{zx}, Q_{zy}). \end{aligned} \tag{4}$$

3 INVERSION METHOD

The inversion algorithm has been designed to invert MT and/or CSAMT data. The inversion of MT data alone, with the galvanic distortion matrices (eq. 4), is unstable because only the product of the impedance and the galvanic distortion parameters can be recovered. Without any additional information the regional impedance tensor values cannot be obtained. There are some basic differences between controlled source and natural magnetotelluric methods that can help us to understand why the full galvanic decomposition works for CSAMT but not for MT. In controlled source EM methods the real part of the impedance approaches an asymptote at long periods and never vanishes. In the same way the tipper vector approaches a finite constant at long periods. The long period range where these effects occur is called the *near field*, and primarily provides information concerning the source and receiver, although it must also be related to the conductivity of the medium through the electric fields. The use of the *near field* provides extra information that makes the full galvanic decomposition possible, providing more degrees of freedom for the inverse problem.

The inversion algorithm is based on that described by Pedersen & Rasmussen (1989) and is modified to include the inversion of CSAMT. The model and data are parametrized in the following way: the impedance tensor, $\boldsymbol{Z}$, and the tipper vector, (A, B), that are measured in periods T_k $(k = 1, \ldots, N)$, M are the number of layers of the model, and N is the total number of observations represented by the vector $\mathbf{y}$:

$$\begin{aligned}\mathbf{y}^{\mathrm{T}} = \big(&\Re\left(Z^1_{xx}\right), \Im\left(Z^1_{xx}\right), \Re\left(Z^1_{xy}\right), \Im\left(Z^1_{xy}\right),\\ &\Re\left(Z^1_{yx}\right), \Im\left(Z^1_{yx}\right), \Re\left(Z^1_{yy}\right), \Im\left(Z^1_{yy}\right),\\ &\Re(A^1), \Im(A^1), \Re(B^1), \Im(B^1),\\ &\Re\left(Z^2_{xx}\right), \Im\left(Z^2_{xx}\right), \Re\left(Z^2_{xy}\right), \Im\left(Z^2_{xy}\right),\\ &, \ldots,\\ &\Re(A^N), \Im(A^N), \Re(B^N), \Im(B^N)\big)^{\mathrm{T}}.\end{aligned} \tag{5}$$

The response vector is defined as

$$\mathbf{f}^{\mathrm{T}} = (f_1, f_2, \ldots, f_N)^{\mathrm{T}}. \tag{6}$$

This model is a function of P parameters that are the elements of a vector θ,

$$\begin{aligned}\boldsymbol{\theta} = (&\ln \rho_1, \ln d_1, \ldots, \ln \rho_{M-1}, \ln d_{M-1}, \ln \rho_M,\\ &P_{xx}, P_{xy}, P_{yx}, P_{yy}, Q_{xx}, Q_{xy}, Q_{yx}, Q_{yy}, Q_{zx}, Q_{zy})^{\mathrm{T}},\end{aligned} \tag{7}$$

where ρ_i and d_i are the resistivity and the thickness of each layer, respectively. The total number of parameters for a layered earth with M layers is thus $P = (2M - 1) + 10$, which are the $2M - 1$ regional model parameters plus the 10 that define the complete galvanic distortion (eq. 4).

For the regional model parameters a logarithmic parametrization has been used, while for the distortion parameters the chosen parametrization has been linear. The logarithmic representation is robust in the sense that it prevents negative values of the apparent resistivities and thicknesses (Pedersen & Rasmussen 1989).

Introducing θ^0_j as an initial estimate of the parameter θ_j, $(j = 1, \ldots, P)$, $\mathbf{f}^0$ as the initial response of the model, and assuming that the response vector is a linear function with respect to the parameters, a perturbation of the response model over $\boldsymbol{\theta}^0$ as a first-order development in Taylor series can be expressed as

$$\mathbf{f} = \mathbf{f}^0 + \sum_{j=1}^{p} \left.\frac{\partial \mathbf{f}}{\partial \theta_j}\right|_{\theta=\theta_0} \left(\theta_j - \theta^0_j\right) = \mathbf{f}^0 + \boldsymbol{J}\delta, \tag{8}$$

where $\boldsymbol{J}$ is the Jacobian matrix of partial derivatives with respect to the parameters and δ is a vector that represents the change in the parameters. The perturbations have to be chosen so that they minimize the square of the sum of the errors between the response model and the data. To this end, an error function that defines the difference between the response of the model, $\mathbf{f}$, and the observed data, $\mathbf{y}$, is introduced:

$$\mathbf{e} = \mathbf{y} - \mathbf{f}. \tag{9}$$

The vector $\boldsymbol{y} - \boldsymbol{f}^0$, which contains the differences between the response of the initial model and the observed data is called the discrepancy vector, $\mathbf{g}$. An error in the estimation of the model for certain parameters can be defined from eqs (8) and (9):

$$\mathbf{e} = \boldsymbol{g} - \boldsymbol{J}\boldsymbol{\delta}. \tag{10}$$

In the least-squares or the Gauss–Newton approximation methods, we try to minimize the quadratic error $S = \mathbf{e}^{\mathrm{T}} \cdot \mathbf{e}$ with respect to the vector change in the parameters, δ. From eq. (10) the following relationship is obtained:

$$S = \mathbf{e}^{\mathrm{T}} \cdot \mathbf{e} = (\boldsymbol{g} - \boldsymbol{J}\boldsymbol{\delta})^{\mathrm{T}}(\boldsymbol{g} - \boldsymbol{J}\boldsymbol{\delta}). \tag{11}$$

The inverse problem is then solved using the singular-value decomposition based on the Marquardt stabilization method. The inversion begins with an iterative process of searching the optimum Marquardt parameter. To do this the algorithm starts with an initial value of the Marquardt parameter equal to the largest eigenvalue, and then modifies it, first decreasing it in smaller intervals for each iteration, then increasing it, until an optimum value has been estimated. After this process, a classical iterative least-squares method is applied until the convergence to a minimum is reached. An accurate description of this method, and the calculation of the misfit and deviation of the model, can be found in Pedersen & Rasmussen (1989).

4 SYNTHETIC MODEL

As an example of the application of this methodology we first present the results from an analysis of a controlled-source sounding located on a layered earth in which a shallow conductive structure has been embedded between the transmitter and the receiver in order to cause galvanic distortion. The response was calculated using a 3-D modelling algorithm that uses integral equations to solve the Green functions numerically (Xiong 1989, 1992a,b). The distortion model used in this test has been expressed as eq. (1). The synthetic model consists of a layered earth consisting of a 100 Ω m layer, over a 10 000 Ω m half-space. The resistivity of the conductor is 0.5 Ω m and is located between the transmitter and the receiver. The geometry of this model is shown in Fig. 1. The transmitter is formed by two orthogonal dipoles of 300 m length and is located at a distance of 1.5 km from the receiver (R). The responses obtained from this 3-D modelling code have been checked with responses from a MT 3-D modelling code (Mackie *et al.* 1994) for the *far-field* solution and the modelling package EMIGMA (see the note in the acknowledgments), obtaining similar responses for the configuration used. For the first test, all the galvanic magnetic distortion and the regional parameters were considered. The algorithm achieved an rms fit below 1 on the first iteration and accordingly stopped. Besides recovering the correct regional model the algorithm also retrieved the following distortion parameters:

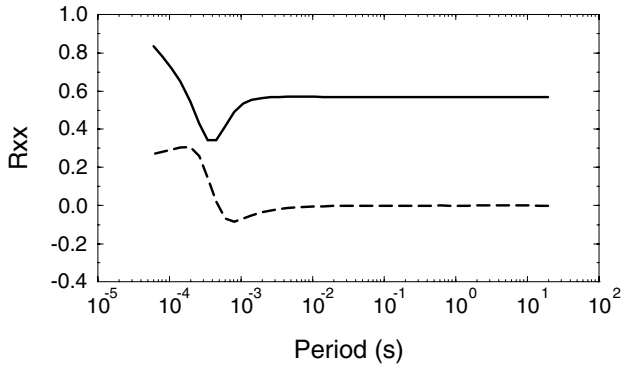

Figure 2. Unique component of the magnetic galvanic distortion matrix that is not zero, corresponding to the model of Fig. 9. For long periods the distortion is frequency independent and non-zero, causing a static shift of the curves. solid line, real part; dashed line, imaginary part.

$$\boldsymbol{P} = \begin{pmatrix} 0.361 & 0.000 \\ 0.000 & 0.003 \end{pmatrix} \pm \begin{pmatrix} 0.025 & 0.010 \\ 0.006 & 0.004 \end{pmatrix}$$

$$\mathbf{Q}_h = \begin{pmatrix} 0.000 & -0.003 \\ 0.408 & 0.000 \end{pmatrix} \pm \begin{pmatrix} 0.003 & 0.002 \\ 0.010 & 0.005 \end{pmatrix} \Omega^{-1}$$

$$\mathbf{Q}_z = \begin{pmatrix} -0.039 \\ 0.000 \end{pmatrix} \pm \begin{pmatrix} 0.005 \\ 0.002 \end{pmatrix}.$$

The distortion body can be considered as 2-D, as it only affects one of the two components of each of the horizontal electromagnetic fields, although this is the result of the symmetry of the problem. This body induces a secondary electric field in the direction across the strike independent of the polarization of the wave. The regional horizontal magnetic field is affected by a magnetic field induced in the distortion body and perpendicular to it (along strike). To observe the effect of the magnetic distortion the R_{xx} component of the magnetic distortion matrix (eq. 3) has been plotted (Fig. 2). Because the regional earth is 1-D the impedance tensor will have zero diagonal elements and a non-zero off-diagonal, and from the fact that the horizontal magnetic distortion has only one non-zero component, it can be deduced that this is the only component of the magnetic distortion matrix (**R**) that does not vanish.

The frequency dependence of the magnetic galvanic distortion is also appreciated in Fig. 2. The sharp variations between 10^4 and 10^3 Hz correspond to the *transition zone*, the stabilization for higher periods caused by the independence on the frequency of the EM fields on the *near field*. The effect of the magnetic galvanic distortion for the controlled-source method at low frequencies is of a static shift, like that caused by the distortion of the electric field. This difference in the behaviour of the magnetic distortion between the natural and controlled-source methods can be explained from a mathematical point of view due to the fact that the impedance tensor approaches an asymptote for long periods for the controlled-source method while for the natural one, the impedance tends to zero. From a physical point of view, the galvanic distorter can be viewed as a local source, because of the close distance to the receiver, the local field will be in the *near field*, thus the local galvanic electric and magnetic fields are frequency independent and their effect will be a static shift.

As can be appreciated (Fig. 2), the effect of the magnetic galvanic distortion on the controlled-source methods can affect severely data at long periods, with the degree of severity depending on the geometry of the problem: the situation of the source, the type of distorting bodies, the regional model, etc. In very resistive basements, such as shields with conductive intrusions and heavily fractured zones, the magnetic distortion can affect the data severely.

For the second test, the same data from test 1 was used, but this time only electric galvanic distortion was considered, and the magnetic galvanic components were equal to 0 and frozen. The best model obtained has an rms fit over 5 and cannot recover the original model parameters. The electric distortion tensor is

$$\boldsymbol{P} = \begin{pmatrix} -0.193 & 0.000 \\ 0.000 & 0.000 \end{pmatrix} \pm \begin{pmatrix} 0.021 & 0.000 \\ 0.010 & 0.002 \end{pmatrix}.$$

As an example of the visual fit of this data, Fig. 3 shows the Z_{xy} and B components of the transfer functions. As can be

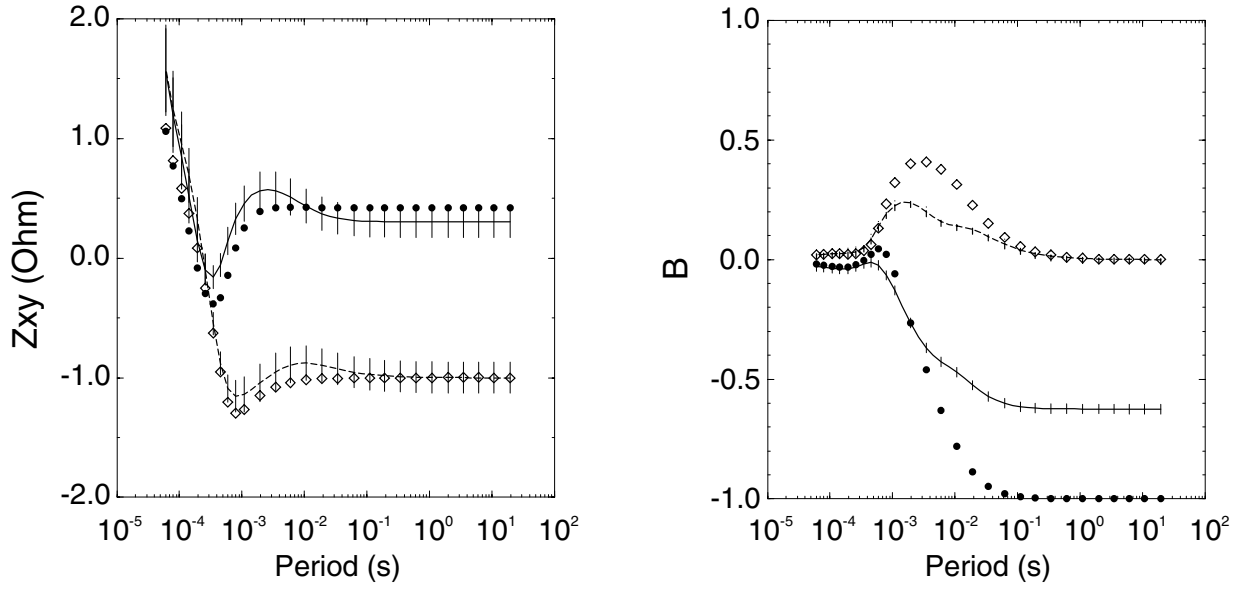

Figure 3. Fit of the Z_{xy} and B components of the transfer functions using an electric galvanic model. ○, real part of the data; ◇, imaginary part of the data; solid line, real part of the model response; dashed line, imaginary part of the model response.

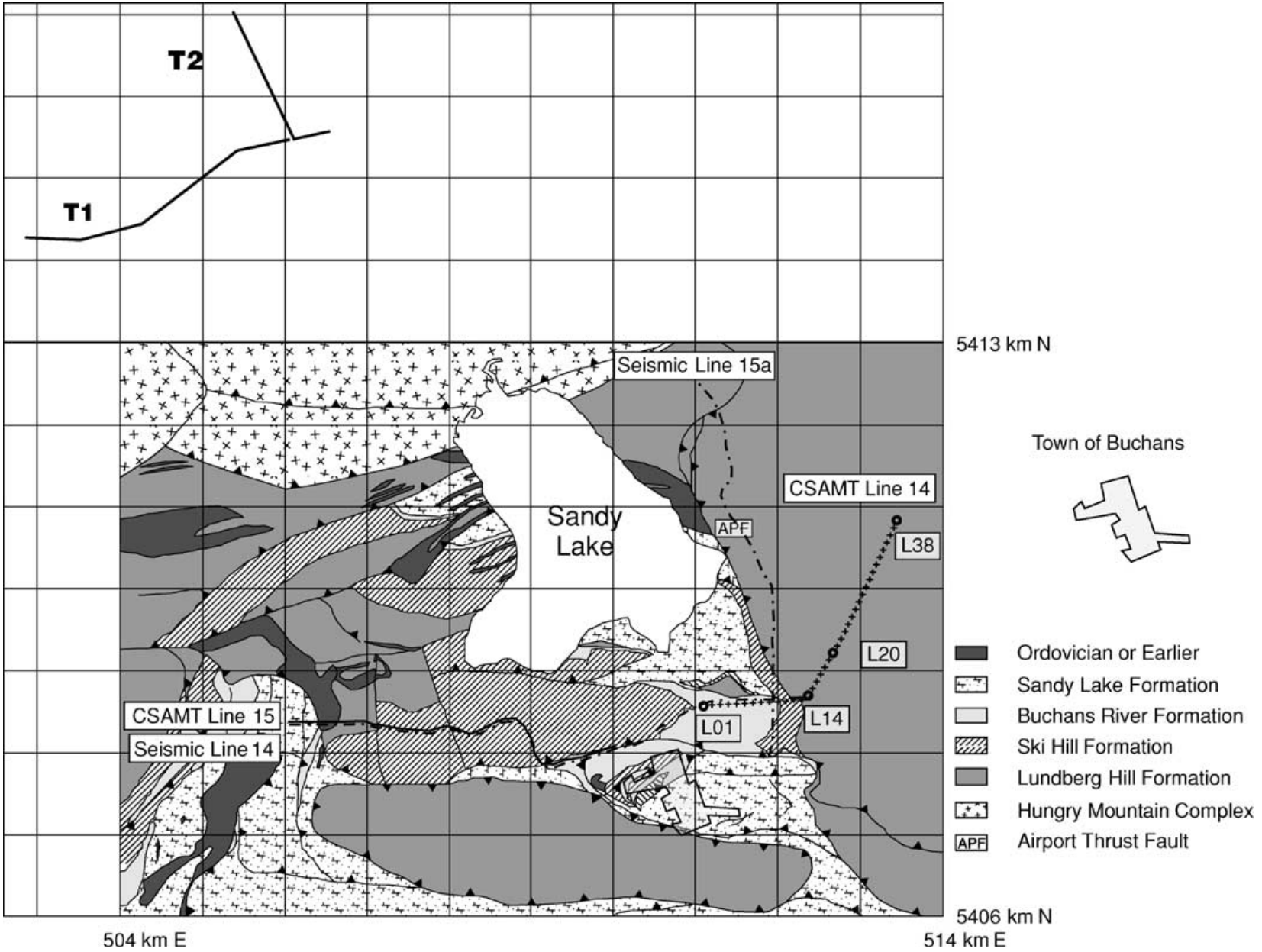

Figure 4. Geological map of the study area showing the position of the existing seismic and CSAMT profiles (lines 14 and 15) and the two orthogonal transmitters (T1 and T2) used for the CSAMT soundings located in the Hungry Mountain Complex. Modified after Thurlow *et al.* (1992).

appreciated the largest misfit is in the *far field* and the *transition zone*.

5 BUCHANS MINE CSAMT DATA

Newfoundland forms part of the Canadian Appalachian Orogen, which is divided into five broad zones. The Lower Ordovician Buchans Group, where the area of study is located, forms part of the Dunnage Zone of Central Newfoundland, a structurally assembled collage of rocks that record the opening and subsequent closure of the Iapetus Ocean during the Late Precambrian–Early Paleozoic. This zone represents vestiges of Iapetus with island arc sequences and mèlanges built upon oceanic crust (Williams 1979). In the Buchans Mine area, four volcano-sedimentary formations were defined by Thurlow & Swanson (1987), each consisting of varying proportions of proximal felsic and mafic volcanic and volcaniclastic rocks that display complex, but well-understood facies interactions characteristic of an active volcanic–tectonic environment. Fig. 4 shows the geological map of the zone together with the seismic and CSAMT profiles. The map also shows the four volcanic sequences (Sandy Lake, Buchans River, Ski Hill and Lundberg formations) and the main faults, intercepted by post-depositional thrust faulting.

A previous CSAMT survey was conducted and interpreted by Boerner *et al.* (1993a,b) some 4 km west of the area of study. The authors determined that the use of the orthogonal components of the horizontal electromagnetic fields was inappropriate for the interpretation of the Earth's conductivity structure, due to the strong scattering in the electric fields. Instead they used the length of the major axes of the electric and magnetic field polarization ellipses and the vertical magnetic field. This definition of the impedance tensor is independent of the coordinate system chosen or of the azimuth of the field components, and it does not require orthogonality in the measured electric and magnetic fields. They also showed that the data can be interpreted using a layered earth model based on the observation that the static (DC) magnetic fields were only dependent on the geometry of the source and receiver, and the distortion of the fields is caused by the presence of local 3-D structures. From the analysis of this static (DC) limit, they conclude that there is a local 3-D structure to transmitter 1. To correct the galvanic distortion they include a new parameter during the inversion of the data to control the static shift. The resistivity model they obtained shows a

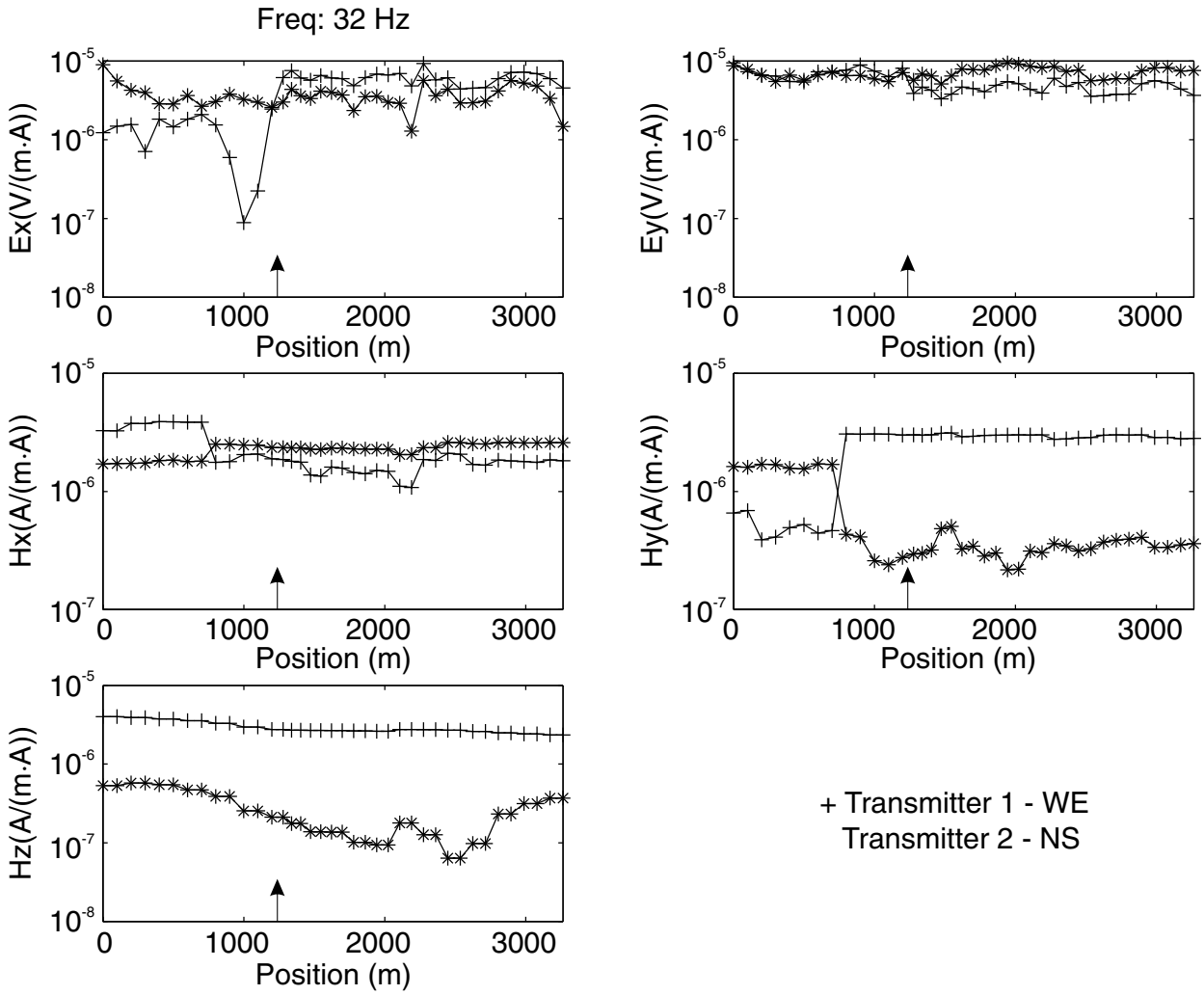

Figure 5. Profiles of the EM fields at 32 Hz. The position of the stations has been calculated as the distance to the first station (L01). The arrow indicates the position of station L14. As can be observed there are local variations between adjacent stations, suggesting galvanic distortion rather than regional inductive effects.

three-layered earth with an electrical contact that dips towards the west, showing at least a 1:3 contrast between the electrical resistivity of the overlying material and the resistive basement.

In Fig. 5 we plot the profiles of the electromagnetic fields at 32 Hz. The jagged shape of the EM fields suggests that the variations between sites are local rather than regional features (2-D or 3-D inductive effects). These local effects have been interpreted as galvanic and the use of the code developed in this study is thus justifiable. Fig. 6 shows the apparent resistivity pseudosections, in which both modes are shown. The TM mode has been defined to be parallel to the profile and the TE mode perpendicular to the profile. The profiles have been divided into two segments because of the different azimuth angles for stations 01 to 13 (segment I) and from 14 to 38 (segment II). As can also be observed in the profile sections of the EM fields (Fig. 5), there is a clear difference in the data from each profile. Segment I shows evidence of lateral continuity until station 07 and 08, with the data showing a constant increase of resistivity with period, after this point there is an increase of the apparent resistivity at short periods and the data shows little variability with period. The contact between segments I and II is marked by the contact between the Ski mountain and the Lundberg mountain units. Therefore, the observed change in the bulk electrical conductivity of the rocks can be caused by the most important geological feature in this zone, the Airport thrust fault (Fig. 7). Segment II shows strong variability of the resistivity between both modes towards its northern part (between stations 30 and 38). Station 24 is marked

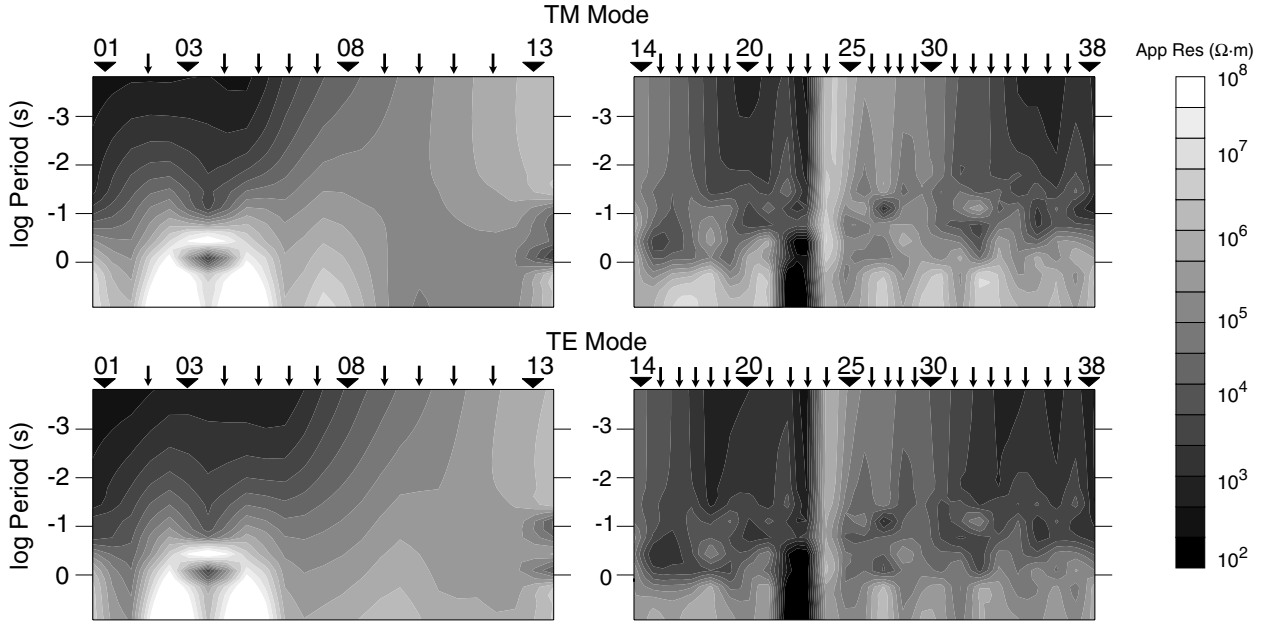

Figure 6. Apparent resistivity pseudosections for the CSAMT line 14. The TM mode has been defined as data along profile while the TE is across profile. On the left-hand side there are the pseudosections form profile I and on the right-hand side for profile II.

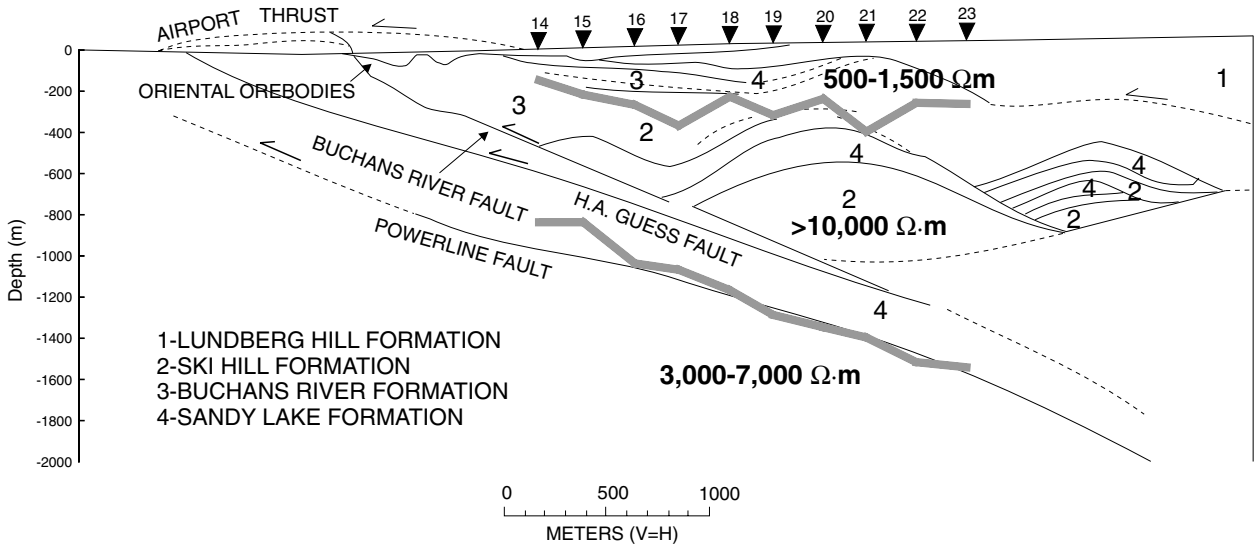

Figure 7. Interpretation of seismic line 15 (Thurlow *et al.* 1992). The CSAMT stations used in this work are indicated on the surface. The CSAMT interpretation is shown as a thick line with the resistivity values indicated between layers.

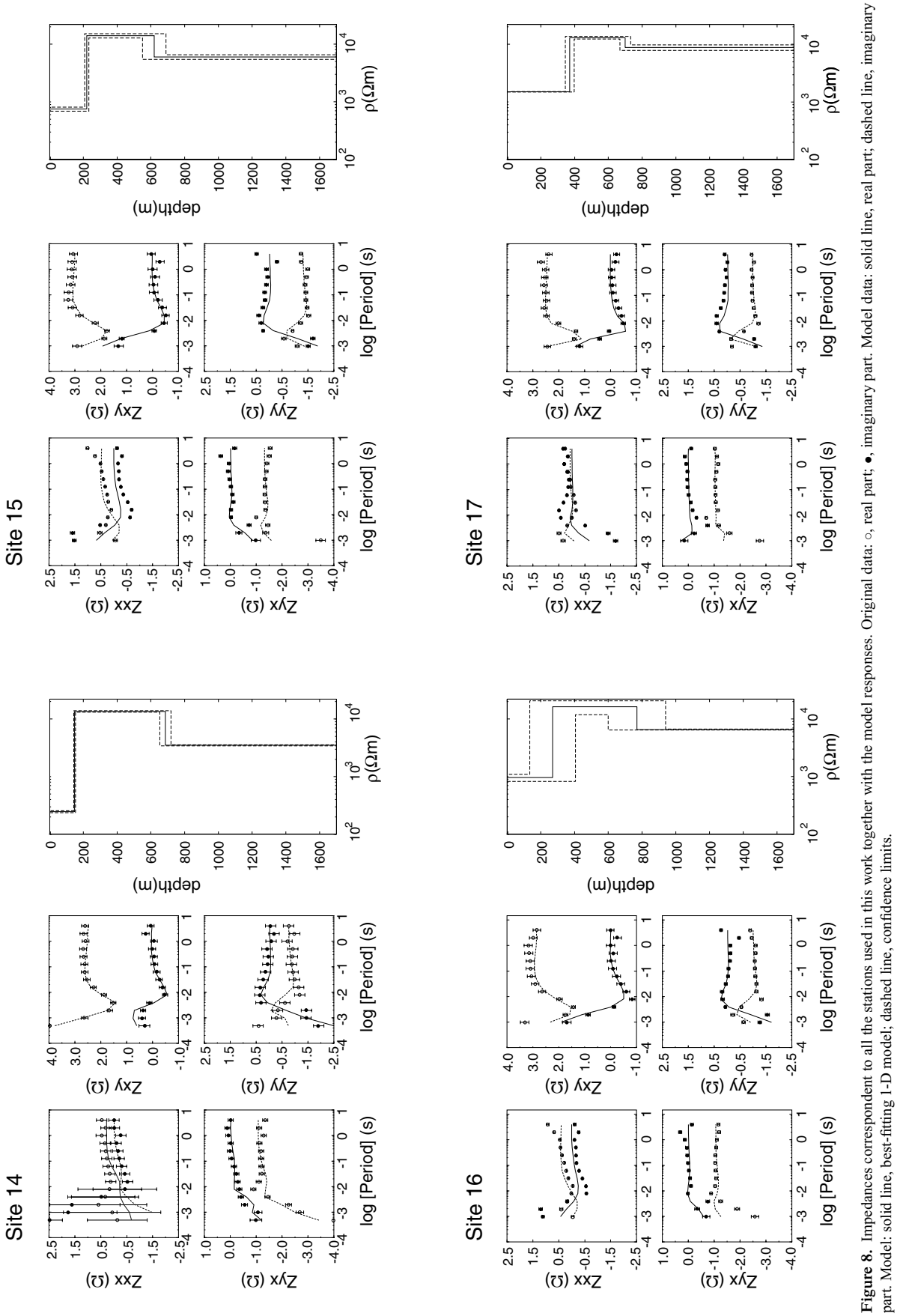

Figure 8. Impedances correspondent to all the stations used in this work together with the model responses. Original data: ○, real part; ●, imaginary part. Model data: solid line, real part; dashed line, imaginary part. Model: solid line, best-fitting 1-D model; dashed line, confidence limits.

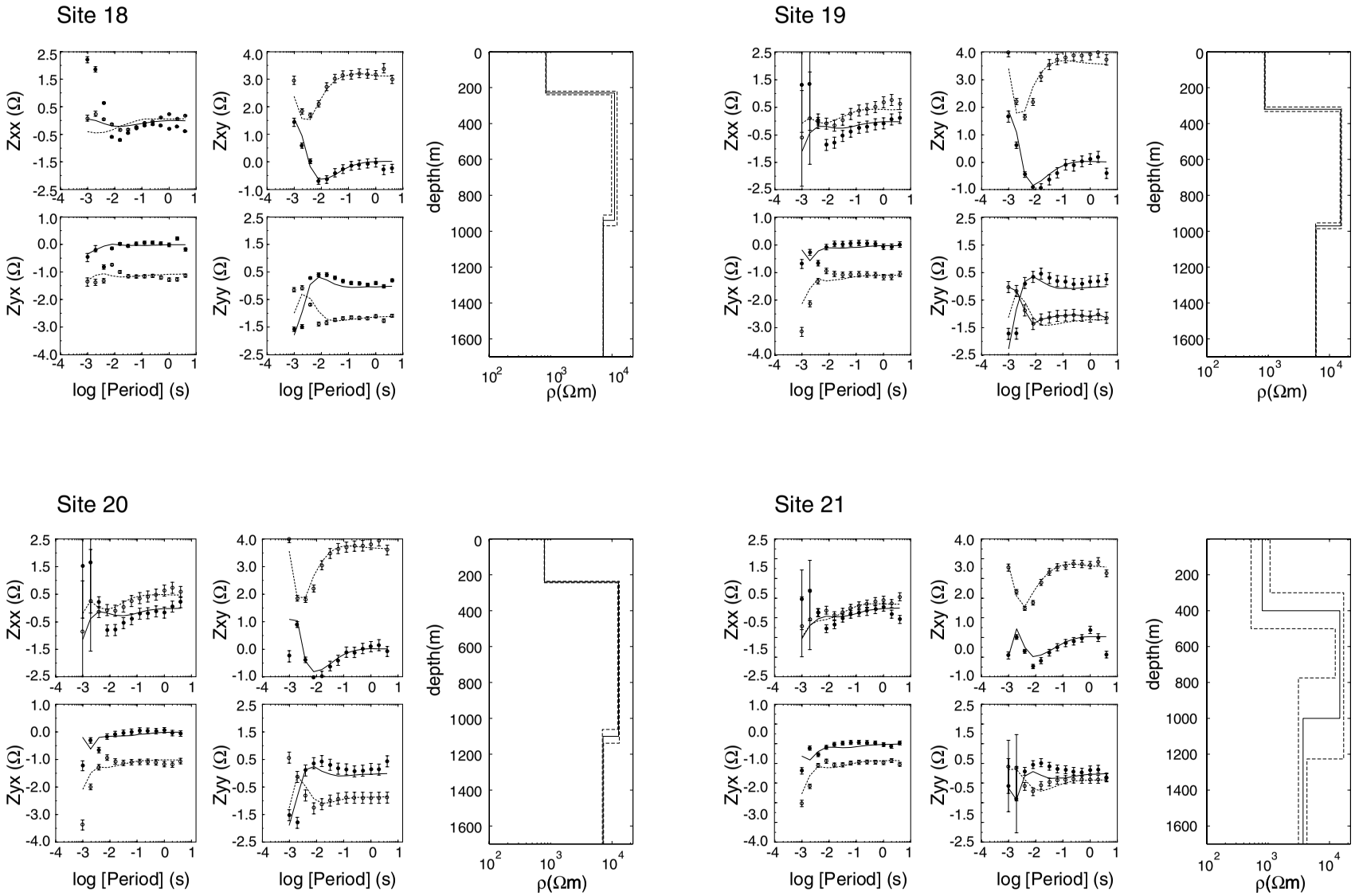

Figure 8. (*Continued.*)

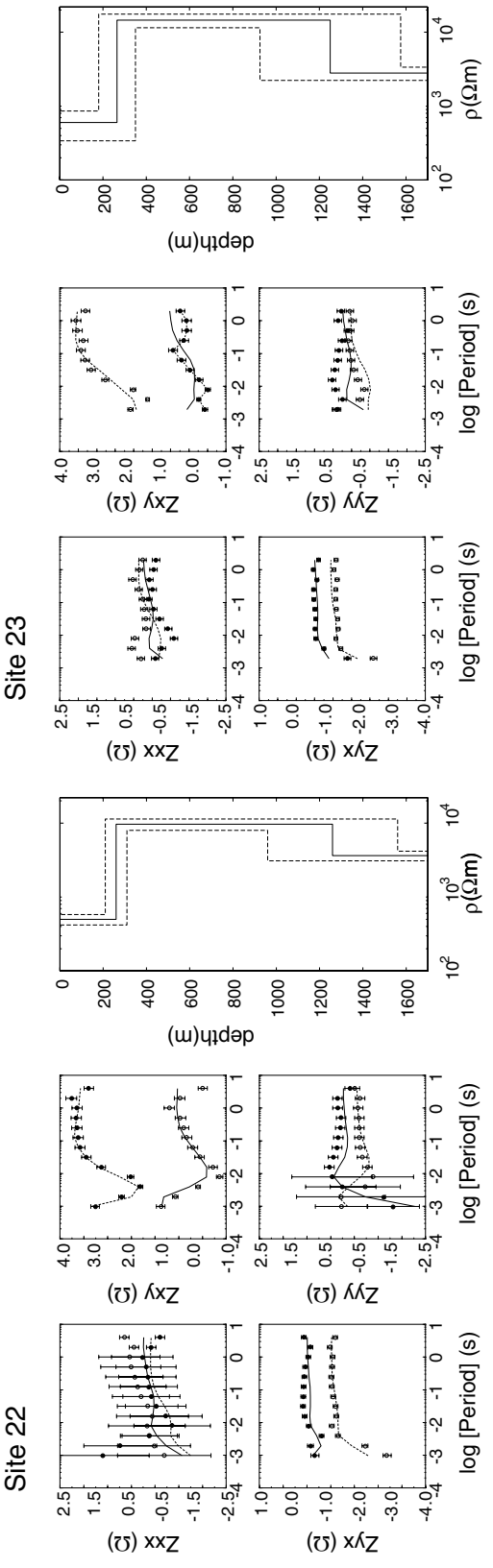

Figure 8. (*Continued.*)

by an increase of the resistivity, reaching 10^6 Ω m and the transition zone is not visible. Southwest of it, from station 23 towards 14, there is a region in which both modes are alike, showing little variability laterally. Stations 23 and 22 show a decrease in resistivity for long periods, which is caused by a drop of the curves (Fig. 8b), probably caused by noise.

The vertical magnetic field transfer functions have not been used in this work. At most of the stations the amplitude of the vertical component was larger than the horizontal components. This data set is very noisy towards the end of the profile (stations 22–38), displaying scattered points or big drops or increases of amplitude. This can be caused by problems during acquisition of data and noise sources. In the analysis of line 15, Boerner *et al.* (1993a) suggested that the reason for the model failing to explain the data could be due either to strong distortion effects or to deviations from 1-D regional structure. In that study, the authors suggested that the noise present in the data they analysed can be caused by the proximity of the town of Buchans, the mining activity present in the area or to nearby metallic pipes. The data analysed in this study (line 14) may also be affected by the same noise sources. Because the Buchans units are highly resistive, this implies that non-uniform fields may be enhanced, thus distorting the regional plane wavefields (Jones 1980). The data used in this work was never analysed, in part because of their poor quality. Two factors help us obtain a valid conductivity model: there are two sources available and thus we can define an impedance tensor with the possibility of applying rotations, and secondly the use of a galvanic decomposition method, including electric and magnetic distortions.

6 CONDUCTIVITY MODEL

All 38 stations that comprise the line 14 CSAMT survey were inverted using the algorithm described earlier. Of those, only 10 (stations 14–23) could be inverted successfully, and these results have been used to obtain the conductivity model that we present here.

As a result of the proximity of line 15 to our data, the model of Boerner *et al.* (1993a) has been used as an initial model for each individual inversion of the stations from line 14. The inversion procedure consisted of successive inversions of the data using the best model from every inversion as a starting model for the new inversion. The final model was obtained when the error could not be improved. Fig. 7 shows the resistivity model together with the seismic and geological models (Thurlow *et al.* 1992). The model consists of a three-layered earth, showing a modest conducting upper layer with a resistivity range from 500 to 1500 Ω m, overlying a resistive layer (>10 000 Ω m) dipping northeast, and a basal layer with a resistivity range between 3000 and 7000 Ω m. Fig. 8 shows the fit of the inverted model response to the observed data for all the stations, together with the three-layered model obtained, and in Table 1 there are the inversion model parameters for each site. In general the data is well fitted and it should be noted that a layered (1-D) model has been assumed and that the area is very noisy.

A measure of the sensitivity of the model can be realized through eigenvector/eigenvalue analysis. For this analysis, the eigenvectors obtained from the singular-value decomposition used in the inversion are sorted in decreasing order of their corresponding eigenvalues (λ). Each component of the eigenvector is related to combinations of the inversion parameters, thus eigenvector components with high eigenvalues imply good resolution for the parameters

Table 1. Results from the 1-D inversion of CSAMT data for a three-layered earth model. ρ, resistivity; d, thickness.

Station		Layer 1	Layer 2	Layer 3	rms
14	ρ (Ω m)	247. ± 10.1	13 500. ± 370.	3490. ± 69.8	1.442
	d (m)	148. ± 5.4	686. ± 33.		
15	ρ (Ω m)	750. ± 60.	14 000. ± 1200.	6000. ± 560.	4.935
	d (m)	220. ± 12.	620. ± 70.		
16	ρ (Ω m)	960. ± 135.	16 250. ± 4400.	6550. ± 1300.	4.787
	d (m)	270. ± 66.	770. ± 170.		
17	ρ (Ω m)	1500. ± 15.	13 000. ± 715.	8800. ± 982.	5.339
	d (m)	371. ± 26.	700. ± 32.		
18	ρ (Ω m)	840. ± 10.	11 000. ± 1130.	7200. ± 175.	5.584
	d (m)	230. ± 10.	940. ± 30.		
19	ρ (Ω m)	880. ± 13.	15 300. ± 340.	6000. ± 50.	1.628
	d (m)	320. ± 10.	970. ± 16.		
20	ρ (Ω m)	791. ± 5.4	12 774. ± 396.	7136. ± 163.	1.783
	d (m)	240. ± 4.1	1100. ± 38.		
21	ρ (Ω m)	800. ± 275.	14 700. ± 2280.	3700. ± 580.	1.687
	d (m)	400. ± 100.	1000. ± 226.		
22	ρ (Ω m)	500. ± 80.	9695. ± 1700.	3640. ± 550.	1.615
	d (m)	260. ± 50.	1260. ± 300.		
23	ρ (Ω m)	600. ± 260.	14 545. ± 3030.	2800. ± 573.	2.812
	d (m)	265. ± 85.	1250. ± 325		

associated with those components, while eigenvector components with low eigenvalues mean that the associated parameter combinations are poorly resolved and additional information will be required to determine them. Fig. 9 shows an example of this eigenvector analysis corresponding to the analysis of station 14. The eigenvector analysis reveals that the best resolved parameters for station 14 are the resistivities of the model, while the worst determined is the thickness of the second layer. This feature changes for the rest of the stations, but for most of them the resistivities and the electric galvanic parameters remain the best resolved parameters.

The change between the second and the third layer is coincident with the depth of the Powerline fault. The first layer is highly weathered and fractured, and therefore difficult to associate with any structure. The most plausible explanation for the variability in the resistivity at depth is that the basaltic structures are known to be highly fractured. The presence of minerals or fluids within these fractures could thus enhance the bulk conductivity of one particular thrust sheet.

The Powerline fault occurs at a discontinuity in electrical resistivity. The character of rocks that occur structurally below the Powerline fault is poorly known (Thurlow *et al.* 1992). The interpretation of the CSAMT line 15 (Boerner *et al.* 1993a,b) is that the third layer is more resistive than the second one, suggesting less bulk fracturing structurally below the Powerline fault. In the model obtained in the present work the interpretation is the opposite, suggesting that west of the Airport Thrust, the thrust sheet overlying the Powerline fault is more fractured and thus more conductive relative to the footwall. This difference may be related to the thrust sheet geometry, which is much more complex near CSAMT line 14, resulting in more severe imbrication (and fracturing) of the Sandy Lake Formation.

7 GALVANIC MAGNETIC DISTORTION

In this section we analyse the effect of the magnetic component of the galvanic distortion. Fig. 10 shows the horizontal magnetic galvanic distortion parameters R_{ij} obtained from the analysis of station 14. This corresponds to the distortion caused by the local or secondary

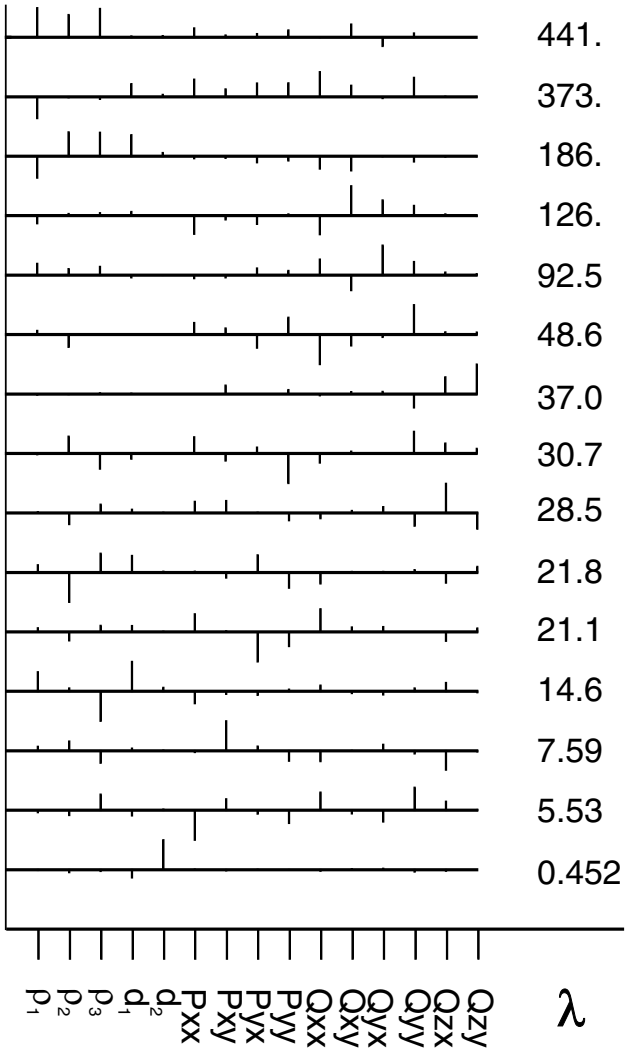

Figure 9. The sensitivity analysis for the model obtained has been realized studying the eigenvectors and eigenvalues correspondent to the inversion problem. The figure shows the analysis for station 14. The most poorly resolved parameter is the thickness of the second layer, and the best resolved parameters are the resistivities of the three layers.

magnetic field related to the electrical charges that accumulated on near-surface structures.

The magnetic galvanic parameters obtained for all stations have the same behaviour, showing a strong frequency dependence at high frequencies. In the *near-field* limit ($f > 90$ Hz) the real part is non-zero and frequency independent, while the imaginary part vanishes, causing a static shift of the apparent resistivity curves that will add to that created by the galvanic distortion of the electric field. As shown in the previous example in which a synthetic data has been analysed using the methodology developed in this paper, the use of simple electric galvanic decomposition on data affected by both electric and magnetic distortion effects, will not recover the regional parameters with a reasonable data fit. The data from line 14 have also been inverted using the 1-D algorithm, but without including magnetic galvanic distortion. An in the synthetic example, the results were unsatisfactory, with responses that failed to reproduce the observed data.

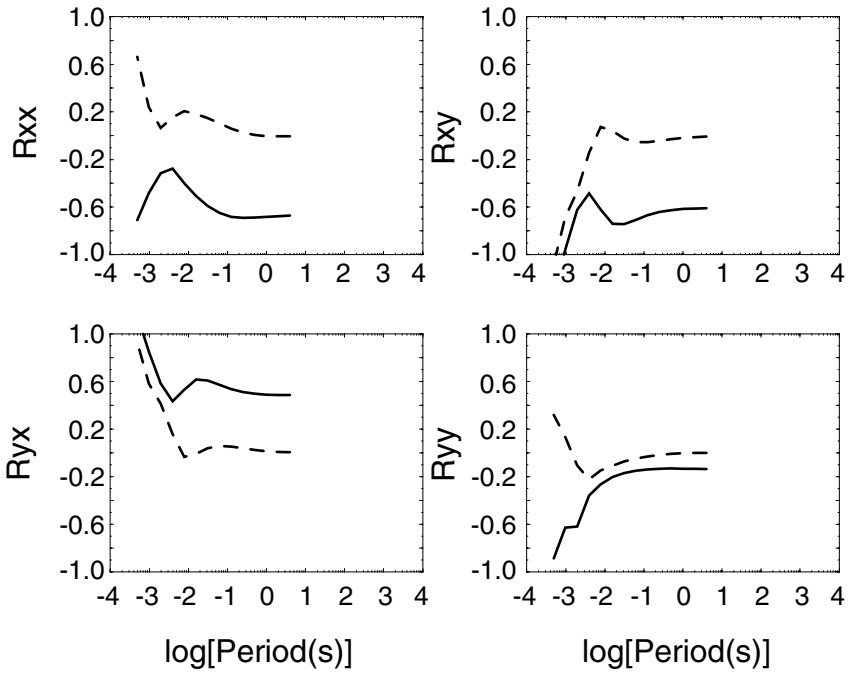

Figure 10. Galvanic magnetic distortion parameters obtained for station 14. The solid line shows the real part, while the dashed line shows the imaginary part. As can be observed, the magnetic distortion parameters are strongly dependent on frequency for high frequencies, and frequency independent for the lowest frequencies. The real parts do not vanish at low frequencies, suggesting that the magnetic distortion at low frequencies causes a static shift that should be added to that caused by the electric galvanic distortion.

8 CONCLUSIONS

Using a simple inversion technique and the basic galvanic distortion equations we have derived a method to recover the regional parameters for 1-D CSAMT data that is severely affected by galvanic distortion. Using this algorithm we inverted CSAMT data from the Buchans mine and recovered a regional model that correlates with the local geology and the results of a coincident seismic reflection survey. The regional model is a three-layer earth and the interface between the second and third layers is coincident with the Powerline fault. Boerner *et al.* (1993a) found that this fault demarcates a change in the electrical properties of the Sandy Lake rocks. As shown in the present work this change extends to the east of the Buchans Mine, adding constraints to the geology of the area.

One of the main conclusions of this work is that in the electromagnetic exploration of shallow structures, magnetic galvanic distortion should be accounted for, especially when using grounded controlled-source methods in which the impedances do not vanish at low frequencies.

ACKNOWLEDGMENTS

WHOI publication number 10773. LITHOPROBE publication number 1215. This work was carried out while XG was a visiting student at the Department of Earth Sciences in Uppsala and at the Geological Survey of Canada in Ottawa. XG was supported by a fellowship of the Spanish Ministry of Science: PB92-0808. Comments by Juanjo Ledo, Pilar Queralt, Jim Craven, Rob Evans, Phil Wannamaker, an anonymous reviewer and the editor, Martyn Unsworth, are also thanked. We are grateful to Zhonghou Xiong for allowing us to use his code. EMIGMA is a 3-D electromagnetic modelling software created by PetRosEikon.

REFERENCES

Boerner, D.E., Wright, J.A., Thurlow, J.G. & Reed, L.E., 1993a. Tensor CSAMT studies at the Buchans Mine in central Newfoundland, *Geophysics,* **58,** 12–19.

Boerner, D.E., Kurtz, R. & Jones, A.G., 1993b. Orthogonality in CSAMT and MT measurements, *Geophysics,* **58,** 924–934.

Chave, A.D. & Smith, J.T., 1994. On electric and magnetic galvanic distortion tensor decompositions, *J. geophys. Res.,* **72,** 4669–4682.

Jones, A.G., 1980. Geomagnetic studies in Scandinavia. I. Determination of the inductive response function from the magnetometer array data, *J. Geophys.,* **48,** 181–194.

Li, X. & Pedersen, L.B., 1991. Controlled source tensor magnetotellurics, *Geophysics,* **56,** 1456–1461.

Li, X., Oskooi, B. & Pedersen, L.B., 2000. Inversion of controlled-source tensor magnetotelluric data for a layered earth with azimuthal anisotropy, *Geophysics,* **65,** 452–464.

Mackie, R.L, Smith, T.J. & Madden, T.R., 1994. Three-dimensional electromagnetic modeling using finite differences equations: the magnetotelluric example, *Radio Sci.,* **29,** 923–935.

Pedersen, L.B. & Rasmussen, T.M., 1989. Inversion of magnetotelluric data: a non-linear least-squares approach, *Geophys. Prospect.,* **37,** 669–695.

Qian, W. & Pedersen, L.B., 1992. Near-surface distortion effects on controlled-source magnetotelluric transfer functions, *Geophys. J. Int.,* **108,** 833–847.

Singer, B.S., 1992. Correction for distortions of magnetotelluric fields, limits of validity of the static approach, *Surv. Geophys.,* **13,** 309–340.

Smith, J.T., 1997. Estimating galvanic-distortion magnetic fields in magnetotellurics, *Geophys. J. Int.,* **130,** 65–72.

Strangway, D.W., Swift, C.M. & Holmer, R.C., 1973. The application of audio-frequency magnetotellurics (AMT) to mineral exploration, *Geophysics,* **38,** 1159–1175.

Thurlow, J.G. & Swanson, E.A., 1987. Stratigraphy and structure of the Buchans Group, in *Buchans Geology, Newfoundland,* ed. Kirkham, R.V., Geological Survey of Canada, Paper 86-24, 35–46.

Thurlow, J.G., Spencer, C.P., Boerner, D.E., Reed, L.E. & Wright, J.A., 1992. Geological interpretation of data from a high resolution reflection survey at the Buchans mine, Newfoundland, *Can. J. Earth Sci.,* **29,** 2022–2034.

Wannamaker, P.E., Hohmann, G.W. & Ward, S.H., 1984. Magnetotelluric responses of three-dimensional bodies in layered earths. *Geophysics,* **49,** 1517–1533.

Williams, H., 1979. Appalachian orogen in Canada, *Can. J. Earth Sci.,* **16,** 792–807.

Xiong, Z., 1989. Electromagnetic fields of electric dipoles embedded in a stratified anisotropic earth, *Geophysics,* **54,** 1643–1646.

Xiong, Z., 1992a. Symmetric properties of the scattering matrix in 3-D electromagentic modeling using the integral equation method, *Geophysics,* **57,** 1199–1202.

Xiong, Z., 1992b. Electromagnetic modeling of 3-D structures by the method of system iteration using integral equations, *Geophysics,* **57,** 1556–1561.

Zhang, P., Roberts, R.G. & Pedersen, L.B., 1987. Magnetotelluric strike rules, *Geophysics,* **52,** 267–278.

Zhang, P., Pedersen, L.B., Mareschal, M. & Chouteau, M., 1993. Channelling contribution to tipper vectors: a magnetic equivalent to electrical distortion, *Geophys. J. Int.,* **113,** 693–700.

Zonge, K.L. & Hughes, L.J., 1991. Controlled source audio-frequency magnetotellurics, in *Electromagnetic Methods in Applied Geophysics,* Vol. 2, pp. 713–809, ed. Nabighian, M.N., Soc. Expl. Geophys., Tulsa, OK.